DOI:10.31557/APJCC.2026.11.6.825

RESEARCH ARTICLE

LncRNA *MALAT1* Promotes Non-Small Cell Lung Cancer Progression by Regulating *FUT4* Expression and EGFR Glycosylation via the PI3K/Akt Pathway

Mohammed Alshwmi[1], Shijun Li[1]*, Muhammad Saleem[2], Gu Juebin[1], Wang Yingxin[1], Mohamed Badheeb[3], Faisal Mohammed Ahmed[4]

[1]Department of Clinical Laboratory, Dalian Medical University, Dalian, Liaoning, People's Republic of China. [2]Department of Pathology and Pathophysiology, College of Basic Medical Sciences, Dalian Medical University, Dalian, Liaoning, People's Republic of China. [3]Department of Internal Medicine, Yale New-Haven Health/Bridgeport Hospital, Bridgeport, CT, USA. [4]Department of Urology, School of Medicine, Ibb University, Ibb, Yemen.

Abstract

Introduction: Lung cancer remains a leading cause of global cancer-related mortality, with non-small cell lung cancer (NSCLC) accounting for approximately 85% of cases. Despite advances in surgery, chemotherapy, and immunotherapy, the molecular drivers of metastasis are still poorly understood. This study investigates the oncogenic role of the long non-coding RNA metastasis-associated lung adenocarcinoma transcript 1 (MALAT1) and its regulation of fucosyltransferase 4 (*FUT4*) in NSCLC progression. **Materials and Methods:** Expression levels of *MALAT1* and *FUT4* were analyzed in 19 pairs of NSCLC tissues and 50 serum samples (15 healthy controls, 20 treatment-naïve patients, and 15 post-chemotherapy patients) using quantitative real-time polymerase chain reaction (RT-qPCR) and enzyme-linked immunosorbent assay (ELISA). The clinical significance of these markers was evaluated in relation to TNM stage and lymph node metastasis. *In vitro* functional assays, including Cell Counting Kit-8, colony formation, and Transwell assays, were performed in A549 and H1299 cells following MALAT1 knockdown or *FUT4* overexpression. All experiments were conducted in three independent biological replicates. Mechanistic insights were obtained using Western blotting, immunoprecipitation, and lectin blotting to assess epidermal growth factor receptor (EGFR) α1,3-fucosylation and phosphatidylinositol 3-kinase (PI3K)/Akt signaling. **Results:** *MALAT1* and *FUT4* were significantly upregulated in NSCLC tissues and serum compared to controls ($P = 0.023$ and $P = 0.017$ for tissue; $P = 0.008$ and $P = 0.011$ for serum, respectively). Spearman correlation analysis revealed a significant positive relationship between *MALAT1* and *FUT4* expression in both tissue ($r = 0.509$; 95% CI: 0.182–0.742; $P = 0.008$) and serum samples ($r = 0.627$; 95% CI: 0.432–0.768; $P < 0.001$). High expression levels were associated with advanced clinical stage and lymph node metastasis ($P = 0.006$ and $P < 0.001$, respectively; these associations should be considered exploratory given the cohort size). Knockdown of *MALAT1* significantly inhibited cell proliferation, migration, and invasion ($P < 0.01$ for all assays). Mechanistically, *MALAT1* regulated *FUT4* expression – potentially through a microRNA-sponging mechanism (a hypothesis requiring direct experimental validation) which in turn mediated α1,3-fucosylation and Lewis Y biosynthesis on EGFR. Reduced *MALAT1* expression led to diminished EGFR activation and subsequent inactivation of the PI3K/Akt/phosphoinositide-dependent kinase signaling cascade ($P < 0.05$). *FUT4* overexpression partially rescued the malignant phenotype and signaling activity suppressed by *MALAT1* silencing ($P < 0.05$ vs. si-*MALAT1* alone), suggesting that additional effectors may contribute to *MALAT1*-dependent phenotypes. **Conclusions:** This study provides evidence that *MALAT1* promotes the malignant progression of NSCLC by modulating the *FUT4*/EGFR/PI3K/Akt signaling axis. These findings highlight *MALAT1* and *FUT4* as potential diagnostic biomarkers and therapeutic targets; however, further validation in larger cohorts and in vivo models is required to establish clinical utility and to elucidate the precise regulatory mechanism linking *MALAT1* to *FUT4* expression.

Keywords: MALAT1- *FUT4*- α1,3-fucosylation- Lewis Y antigen

Asian Pac J Cancer Care, **11 (6)**, 825-839 Submission Date: 07/12/2026 Acceptance Date: 09/02/2026

Corresponding Author:
Professor Shijun Li
Department of Clinical Laboratory, Dalian Medical University, 222 Zhongshan Road, Xigang District, Dalian 116011, Liaoning, People's Republic of China.
Email: lishijun@dmu.edu.cn

Introduction

Lung cancer remains the leading cause of cancer-related mortality worldwide, with non-small cell lung cancer (NSCLC) accounting for approximately 85% of all lung malignancies [1]. Recent global statistics indicate that the incidence and mortality rates of lung cancer continue to pose a significant public health challenge, underscoring the urgency of identifying novel molecular drivers [2]. Current clinical management of NSCLC involves a multidisciplinary approach, including surgical treatment for early-stage patients and comprehensive radiotherapy and chemotherapy for those with advanced disease [3,4]. Although the advent of molecular targeted therapies and immunotherapies has significantly improved survival for selected cohorts, the 5-year survival rates for advanced NSCLC remain low due to therapeutic resistance and disease recurrence [3,5].

The complexity and heterogeneity of NSCLC highlight the urgent need for novel molecular biomarkers and targeted therapeutic strategies [6,7]. To address these challenges, complementary approaches, including those informed by Traditional Chinese Medicine and the study of biological macromolecules, are being extensively evaluated to enhance therapeutic efficacy and minimize treatment-related toxicity [8,9].

Long non-coding RNAs (lncRNAs), defined as transcripts longer than 200 nucleotides that do not encode proteins, have emerged as critical regulators of gene expression through diverse mechanisms, including transcriptional and post-transcriptional modulation and epigenetic regulation [10,11]. Their versatile functions enable lncRNAs to act as oncogenes or tumor suppressors in a highly context-dependent manner, shaping the tumor microenvironment and influencing cancer progression [12,13]. Among these, *MALAT1* (Metastasis-associated lung adenocarcinoma transcript 1), also known as NEAT2, is a phylogenetically conserved lncRNA pathologically overexpressed in various solid malignancies, including lung, gastric, bladder, and breast cancers [14-17]. *MALAT1* upregulation is consistently associated with aggressive clinical phenotypes, increased proliferation, metastatic potential, and poor prognosis. Mechanistically, *MALAT1* promotes epithelial-mesenchymal transition (EMT), a key prerequisite for metastasis, and its silencing reduces NSCLC cell migration, proliferation, and tumor progression in vivo, highlighting its oncogenic potential [17,18]. Alterations in glycosylation patterns, particularly fucosylation, modulate cancer cell behavior and signaling. Fucosyltransferase 4 (*FUT4*) is an enzyme that catalyzes the transfer of fucose in α1,3-linkages to glycoproteins and glycolipids, including the biosynthesis of the tumor-associated Lewis Y (LeY) antigen. *FUT4*-mediated fucosylation regulates essential cellular processes such as adhesion, migration, and signal transduction, and its overexpression is associated with EMT, proliferation, and metastasis in several cancers [14,19]. Notably, LeY antigen modification of the epidermal growth factor receptor (EGFR) enhances receptor activation, contributing to more migratory and invasive cellular phenotypes [20].

Although individual studies have implicated *MALAT1* in NSCLC progression and *FUT4* in glycosylation-mediated signaling, the functional and mechanistic connection between these two molecules in lung cancer remains unexplored. Specifically, whether *MALAT1* exerts its oncogenic effects through regulation of *FUT4*-dependent EGFR glycosylation, and the subsequent impact on PI3K/Akt signaling, has not been investigated. Emerging evidence suggests a potential regulatory relationship between *MALAT1* and *FUT4*. Based on studies in other cancer types [21], it is plausible that *MALAT1* may function as a competitive endogenous RNA (ceRNA) to sequester specific microRNAs, thereby influencing *FUT4* expression. However, this mechanism remains hypothetical in the context of NSCLC and requires direct experimental validation.

We hypothesized that *MALAT1* promotes NSCLC progression by upregulating *FUT4* expression, leading to enhanced α1,3-fucosylation of EGFR, increased LeY antigen biosynthesis, and subsequent activation of the PI3K/Akt signaling cascade. To test this hypothesis, we established the following objectives: (1) characterize *MALAT1* and *FUT4* expression patterns in clinical NSCLC samples and their correlation with clinicopathological parameters; (2) investigate the functional role of *MALAT1* in regulating NSCLC cell proliferation, migration, and invasion; (3) determine whether *MALAT1* regulates *FUT4* expression; (4) elucidate the impact of the *MALAT1*/*FUT4* axis on EGFR glycosylation and PI3K/Akt signaling; and (5) assess the functional relevance of *FUT4* in mediating *MALAT1*-driven phenotypes through rescue experiments.

This study aims to characterize the expression patterns of *MALAT1* and *FUT4* in clinical NSCLC samples and to delineate the molecular mechanisms by which *MALAT1* regulates *FUT4*-dependent glycosylation, alters EGFR signaling, and promotes NSCLC progression via the PI3K/Akt pathway. Understanding this regulatory axis may identify novel biomarkers and molecular targets for diagnostic and therapeutic intervention in NSCLC, although further validation in larger cohorts and in vivo models is required to establish clinical relevance.

Materials and Methods

Clinical Samples

Nineteen fresh-frozen lung cancer tissue samples and their matched adjacent non-tumorous tissues were collected from patients diagnosed with non-small cell lung cancer (NSCLC) at the First Affiliated Hospital of Dalian Medical University (FAHDMU), Dalian, People's Republic of China, between March 2018 and July 2019. The tissue cohort included 6 patients with stage I disease, 4 with stage II disease, and 9 with stage III disease. No stage IV patients were included in the tissue cohort. Additionally, fifty serum samples were obtained from healthy individuals (n = 15) and NSCLC patients (n = 35). Among the NSCLC patients, 20 were

treatment-naïve (stage I, n = 5; stage II, n = 5; stage III, n = 5; stage IV, n = 5) and 15 were post-chemotherapy patients (originally diagnosed with stage III or IV disease). NSCLC diagnosis was confirmed by histopathological examination. Inclusion criteria for NSCLC patients were: (i) histopathologically confirmed primary NSCLC; (ii) no prior systemic treatment (chemotherapy, radiotherapy, or targeted therapy) before sample collection for the treatment-naïve cohort; and (iii) availability of complete clinicopathological data. Exclusion criteria included: (i) history of other malignancies; (ii) concurrent inflammatory or infectious diseases; and (iii) previous neoadjuvant therapy. For tissue analyses, adjacent non-tumorous lung tissues (>2 cm from the tumor margin) were collected from the same patients and confirmed tumor-free by pathological examination. For serum analyses, healthy controls were individuals without any history of cancer or chronic disease, recruited during routine health check-ups at the same institution during the study period. Detailed clinicopathological characteristics of the patient cohort, including age, gender, smoking history, and TNM stage, are provided in Supplementary Tables 1 and 2. Blood samples were collected in serum separator tubes, allowed to clot for 30 minutes at room temperature, and centrifuged at 1500 × g for 15 minutes at 4°C within 2 hours of collection. Serum was aliquoted and stored at -80°C until analysis. To minimize batch effects, samples were processed in random order, and laboratory personnel performing RT-qPCR and ELISA assays were blinded to clinical information. Sample allocation during experimental procedures was randomized using a computer-generated random number sequence. Written informed consent was obtained from all patients before sample collection. The study was approved by the Ethics Committee of FAHDMU (approval no. YJ-KY-FB-2019-32) and conducted in accordance with the Declaration of Helsinki. Samples were processed in random order to minimize batch effects.

Cell Lines and Culture Conditions

Normal human bronchial epithelial (HBE) cells and NSCLC cell lines A549 and H1299 were obtained from Keygen Biotech Co., Ltd. (Nanjing, China). All cell lines were authenticated by short tandem repeat (STR) profiling within the past four years. Results were cross-checked against the International Cell Line Authentication Committee (ICLAC) and ExPASy Cellosaurus databases to exclude misidentification and cross-contamination. Routine mycoplasma testing by PCR confirmed all cell lines were free of contamination.

Cells were cultured in 90% DMEM/L-15 medium (Gibco, Thermo Fisher Scientific, Cat# 11330-032) supplemented with 10% heat-inactivated fetal bovine serum (FBS; Gibco, Cat# 16140-071) and 1% penicillin-streptomycin (HyClone, Cat# SV30010) at 37°C in a humidified atmosphere with 5% CO_2, following international good cell culture practice (GCCP) guidelines. Passage numbers were kept below 20, and early-passage frozen stocks were used to preserve cellular characteristics.

Transfection

For loss-of-function studies, A549 and H1299 cells were transfected with small interfering RNA targeting *MALAT1* (si-*MALAT1*; sense strand 5′-CCCUCUAAAUAAGGAAUAATT-3′) at a final concentration of 100 nM. For gain-of-function studies, *FUT4* overexpression was achieved using a pcDNA3.1(+) vector containing full-length human *FUT4* cDNA (5′-GCUACUACCACCAACUGAGTT-3′; GenePharma, Shanghai, China) at a concentration of 2 μg per well in 6-well plates. A non-targeting scrambled siRNA and an empty pcDNA3.1(+) vector were used as negative controls for knockdown and overexpression experiments, respectively. Transfection concentrations were optimized based on preliminary dose-response experiments (10–200 nM for siRNA; 0.5–4 μg for cDNA) to achieve maximal target modulation with minimal cytotoxicity, as assessed by trypan blue exclusion (>90%). Transfection was performed at 50–70% confluency with 100 nM siRNA or cDNA according to the manufacturer's protocols using Lipofectamine 2000 reagent (Invitrogen, Thermo Fisher Scientific, Cat# 11668019). Media were replaced after 4–6 hours, and assays were conducted 48 hours post-transfection. Transfection efficiency was verified by RT-qPCR.

ELISA

Serum *FUT4* protein levels were measured using a human *FUT4* ELISA kit (R&D Systems, Cat# DY7149) according to the manufacturer's instructions. Absorbance was read at 450 nm on a Multiskan GO microplate reader (Thermo Fisher Scientific, Cat# 51119000). All samples were assayed in duplicate, and the mean value was used for analysis. The inter-assay and intra-assay coefficients of variation were less than 10% and less than 8%, respectively.

Total RNA was extracted from frozen tissue and cultured cells using the RNeasy Mini Kit (QIAGEN, Cat# 74104) according to the manufacturer's instructions. cDNA synthesis was performed with the QuantiTect Reverse Transcription Kit (QIAGEN, Cat# 205311). miRNA expression was quantified using the mirVana qRT-PCR microRNA Detection Kit (Ambion, Cat# AM1558). *MALAT1* and *FUT4* mRNA were quantified by SYBR Green RT-qPCR (Toyobo Co., Cat# QPK-201) on an ABI 7300 Real-Time PCR system. Before experimental analyses, the stability of candidate reference genes (GAPDH, β-actin, and U6) was evaluated across all sample types (tissues, serum, and cell lines) using geNorm and NormFinder algorithms. GAPDH showed optimal stability in tissue and cell line samples (M-value < 0.5), while U6 demonstrated appropriate stability for serum miRNA analyses. All reference genes used in this study exhibited a coefficient of variation less than 15% across experimental conditions, confirming their suitability for normalization. The cycling program was 95°C for 10 minutes, followed by 40 cycles of 95°C for 15 seconds and 60°C for 60 seconds, with melt curve analysis confirming specificity. All reactions were performed in three independent biological replicates,

with each sample run in technical triplicate. Relative expression was calculated using the ΔΔCq method, normalized to GAPDH or U6 as endogenous controls [22, 23]. The ΔΔCq method was applied only after confirming that amplification efficiencies of target and reference genes were approximately equal (within a 5% difference). Specific primer sequences for *MALAT1*, *FUT4*, and internal controls are listed in Supplementary Table 3.

Cell Proliferation and Colony Formation Assays

Cell viability was evaluated using the Cell Counting Kit-8 (CCK-8; Dojindo, Cat# CK04). Transfected cells and controls were seeded at 3×10^3 cells per well in 96-well plates. After 24 hours, 10 μL of CCK-8 solution was added to each well and incubated for 2 hours at 37 °C. Absorbance at 450 nm was measured daily for four consecutive days. The experiment was repeated in three independent biological replicates, with six technical replicates per group per experiment.

For the colony formation assay, transfected and control cells (1×10^3) were seeded in 6-well plates and incubated for 14 days, with medium changed every three days. Colonies were fixed with 4% paraformaldehyde for 15 minutes, stained with 0.1% crystal violet for 20 minutes, and counted using ImageJ software (National Institutes of Health) with a cutoff of more than 50 cells per colony. Each experiment was conducted in triplicate.

Transwell Migration and Invasion Assays

Cell migratory ability was assessed using Transwell chambers with 8 μm pore-size membranes (Nest, Jiangsu, China). Transfected or control cells (1×10^5) in serum-free medium were seeded in the upper chamber, and 600 μL of RPMI-1640 containing 10% FBS was added to the lower chamber as a chemoattractant. To minimize the confounding effect of differential proliferation on migration and invasion assessments, Transwell assays were conducted over 48 hours, a period during which preliminary experiments confirmed no significant differences in cell viability between experimental groups (assessed by parallel CCK-8 assays at 24 and 48 hours; data not shown). Equal cell numbers were seeded in all groups, and non-migrated cells were carefully removed before staining. After 48 hours of incubation at 37°C, non-migrated cells on the upper membrane surface were removed using cotton swabs. Migrated cells were fixed with 4% paraformaldehyde and stained with 0.1% crystal violet. For invasion assays, Transwell membranes were pre-coated with 50 μL of Matrigel (BD Biosciences, Cat# 354234) diluted 1:8 in serum-free medium and allowed to solidify for 2 hours at 37°C before cell seeding. Cells were counted in ten random microscopic fields at 200× magnification by two independent observers blinded to experimental conditions. Each assay was performed in three independent biological replicates. While these measures minimize proliferation-related confounding, we acknowledge that completely separating migration from proliferation effects is challenging *In vitro*. Therefore, migration and invasion data should be interpreted as integrated measures of cell motility and viability under the assay conditions.

Immunofluorescence Assay

Cells grown on coverslips were fixed with 4% paraformaldehyde for 30 minutes, permeabilized with 0.1% Triton X-100 for 5 minutes, and blocked with 4% BSA for 1 hour at room temperature. Cells were incubated overnight at 4 °C with anti-*FUT4* primary antibody (Proteintech, Cat# 13039-1-AP, 1:50 dilution), followed by TRITC-conjugated secondary antibody (Solarbio, Cat# SLZ0410, 1:100 dilution) for 1 hour at room temperature in the dark. Nuclei were stained with DAPI for 5 minutes. Images were captured using a Nikon Eclipse Ti fluorescence microscope (Nikon Corporation) at 400× magnification. Fluorescence intensity was quantified using ImageJ software from at least 100 cells per condition across three independent experiments.

Immunoprecipitation

Cells were lysed in immunoprecipitation lysis buffer containing protease and phosphatase inhibitor cocktails (Thermo Fisher Scientific, Cat# 87788) and incubated overnight at 4 °C with anti-EGFR antibody (Cell Signaling Technology, Cat# 4267). Normal rabbit IgG (Cell Signaling Technology, Cat# 2729) was used as a negative control to confirm antibody specificity. Immune complexes were captured with protein A/G agarose beads (Santa Cruz Biotechnology, Cat# sc-2003), washed three times with lysis buffer, and eluted with SDS loading buffer by boiling at 95°C for 5 minutes. Samples were then analyzed by western blot.

Western Blot Analysis

Total protein was extracted using RIPA lysis buffer (Solarbio, Cat# R0010) containing a protease and phosphatase inhibitor cocktail (Solarbio, Cat# P1260). Protein concentration was determined with a bicinchoninic acid (BCA) assay kit (Pierce, Cat# 23225). Equal amounts of protein (20 μg per lane) were separated by 10% SDS-PAGE and electrophoretically transferred to polyvinylidene difluoride (PVDF) membranes (Millipore). Membrane transfer efficiency was assessed by Ponceau S staining. Membranes were blocked with 5% (w/v) non-fat dry milk in Tris-buffered saline with 0.1% Tween 20 (TBST) for 2 hours at room temperature.

Subsequently, membranes were incubated overnight at 4°C with specific primary antibodies. All primary antibodies, including their targets, commercial sources, catalog numbers, and dilutions, are listed comprehensively in Supplementary Table 4. Following primary incubation, membranes were washed with TBST three times for 10 minutes each and probed for 1.5 hours at room temperature with horseradish peroxidase (HRP)-conjugated secondary antibodies (anti-rabbit IgG, Cell Signaling Technology, Cat# 7074, 1:5000; or anti-mouse IgG, Cell Signaling Technology, Cat# 7076, 1:5000).

Protein bands were visualized using an enhanced chemiluminescence (ECL) detection kit (Millipore, Cat# WBKLS0500) and imaged using a ChemiDoc XRS+ system (Bio-Rad Laboratories) [24]. Band intensity was

quantified by densitometric analysis using ImageJ software (National Institutes of Health), with the expression of each target protein normalized to that of β-actin. All Western blot experiments were performed with three independent biological replicates. Uncropped, full-length blots are provided in Supplementary Figure 1.

Lectin Blot Analysis

For lectin blot analysis, membranes were blocked with 3% BSA in TBST for 1 hour at room temperature, then incubated with biotinylated Lotus Tetragonolobus Lectin (LTL; Vector Laboratories, Cat# B-1325) at 1:1000 dilution overnight at 4°C. After washing, membranes were incubated with HRP-conjugated streptavidin (Cell Signaling Technology, Cat# 3999) at 1:3000 dilution for 1 hour at room temperature. Detection was performed using ECL as described above. For immunoprecipitation-lectin blot experiments, EGFR was immunoprecipitated as described above, and eluted proteins were subjected to lectin blotting with LTL to detect α1,3-fucosylated glycans specifically on EGFR. Coomassie Brilliant Blue staining of parallel gels was used as a loading control for lectin blots. We acknowledge that the assessment of EGFR glycosylation in this study relies primarily on immunoprecipitation followed by lectin blotting and LeY immunodetection. While these approaches provide evidence of glycosylation status, they do not offer detailed structural information about glycan composition. Future studies employing mass spectrometry-based glycoproteomics would provide complementary, higher-resolution characterization of EGFR glycosylation patterns modulated by the *MALAT1*/*FUT4* axis.

Statistical Analysis

Data represent mean ± standard error (SE) from at least three independent experiments, with each experiment containing technical replicates (as indicated in respective method descriptions). Data distribution was assessed for normality using the Shapiro-Wilk test. For normally distributed data, statistical analyses were performed using Student's t-test (two-tailed) for two-group comparisons or one-way ANOVA with Tukey's post hoc test for multiple comparisons. For non-normally distributed data, the Mann-Whitney U test was used for two-group comparisons, and Kruskal-Wallis test with Dunn's post hoc test was used for multiple comparisons. Spearman's rank correlation was used to evaluate relationships between *MALAT1* and *FUT4* expression due to the non-normal distribution of expression data. For clinicopathological associations, Fisher's exact test was used for categorical variables with small sample sizes, and the chi-square test for trend was used for ordinal variables across stage categories. Effect sizes were calculated as Cohen's d for t-tests and η^2 for ANOVA. For multiple comparisons, the Benjamini-Hochberg procedure was applied to control the false discovery rate at 5%. All analyses were conducted with GraphPad Prism 9.0 (GraphPad Software, Inc.). Exact P values are reported throughout, with values less than 0.0001 denoted as $P < 0.0001$. P-values less than 0.05 were considered statistically significant.

Results

MALAT1 Shows a Positive Correlation with FUT4 Expression in Human Lung Cancer

Analysis of lung cancer tissues (n = 19) and serum samples (n = 50) showed significant upregulation of both *MALAT1* and *FUT4* compared to matched normal controls (Figures 1A, 1B; P = 0.023 for *MALAT1* tissue; P = 0.017 for *FUT4* tissue; P = 0.008 for *MALAT1* serum; P = 0.011 for *FUT4* serum). All qPCR reactions were performed in technical triplicates, and the data represent biological replicates from distinct patient samples. Spearman's rank correlation analysis revealed a significant positive relationship between *MALAT1* and *FUT4* expression levels in tumor tissues (r = 0.509; 95% confidence interval: 0.182–0.742; P = 0.008; Figure 1C). Western blotting confirmed increased *FUT4* protein expression in tumor tissues compared to adjacent normal lung samples (Figure 1D; P = 0.015).

The tissue cohort included 19 NSCLC patients: 6 with stage I disease, 4 with stage II, and 9 with stage III. The serum cohort included 50 participants: 15 healthy controls, 20 treatment-naïve NSCLC patients (stage I, n = 5; stage II, n = 5; stage III, n = 5; stage IV, n = 5), and 15 post-chemotherapy NSCLC patients. Clinical-pathological analysis showed that high expression of *MALAT1* and *FUT4* in serum and tissue was significantly associated with advanced clinical stage (Stages III–IV) and lymph node metastasis (P = 0.006 for clinical stage; P < 0.001 for lymph node metastasis; Supplementary Tables 1 and 2).

Due to the modest sample size of the tissue cohort (n = 19), multivariable logistic regression analysis was not performed to avoid overfitting. Therefore, the associations between marker expression and clinical parameters should be interpreted as exploratory observations that require validation in larger, independent cohorts.

Serum concentrations of *MALAT1* and *FUT4* were significantly decreased in lung cancer patients after chemotherapy compared to untreated individuals (Figures 1E, 1F; P = 0.032 for *MALAT1*; P = 0.028 for *FUT4*). Enzyme-linked immunosorbent assay (ELISA) further confirmed a significant positive correlation between serum *FUT4* protein and *MALAT1* levels (Spearman's r = 0.627; 95% CI: 0.432–0.768; P < 0.001; Figures 1G, 1H). Collectively, these data suggest that *MALAT1* and *FUT4* are concurrently upregulated in non-small cell lung cancer (NSCLC) and highlight their potential as biomarkers for disease severity, warranting further investigation in larger prospective studies.

MALAT1 Promotes Proliferation and Migration in Lung Cancer Cells

In vitro, MALAT1 and *FUT4* expression were significantly elevated in A549 and H1299 NSCLC cell lines compared to normal human bronchial epithelial (HBE) cells (Figures 2A, 2B; P = 0.009 for A549 *MALAT1*; P = 0.013 for A549 *FUT4*; P = 0.006 for H1299 *MALAT1*; P = 0.011 for H1299 *FUT4*). Knockdown of *MALAT1* via siRNA (si-*MALAT1*) significantly inhibited cell proliferation as measured by CCK-8 assay over four days

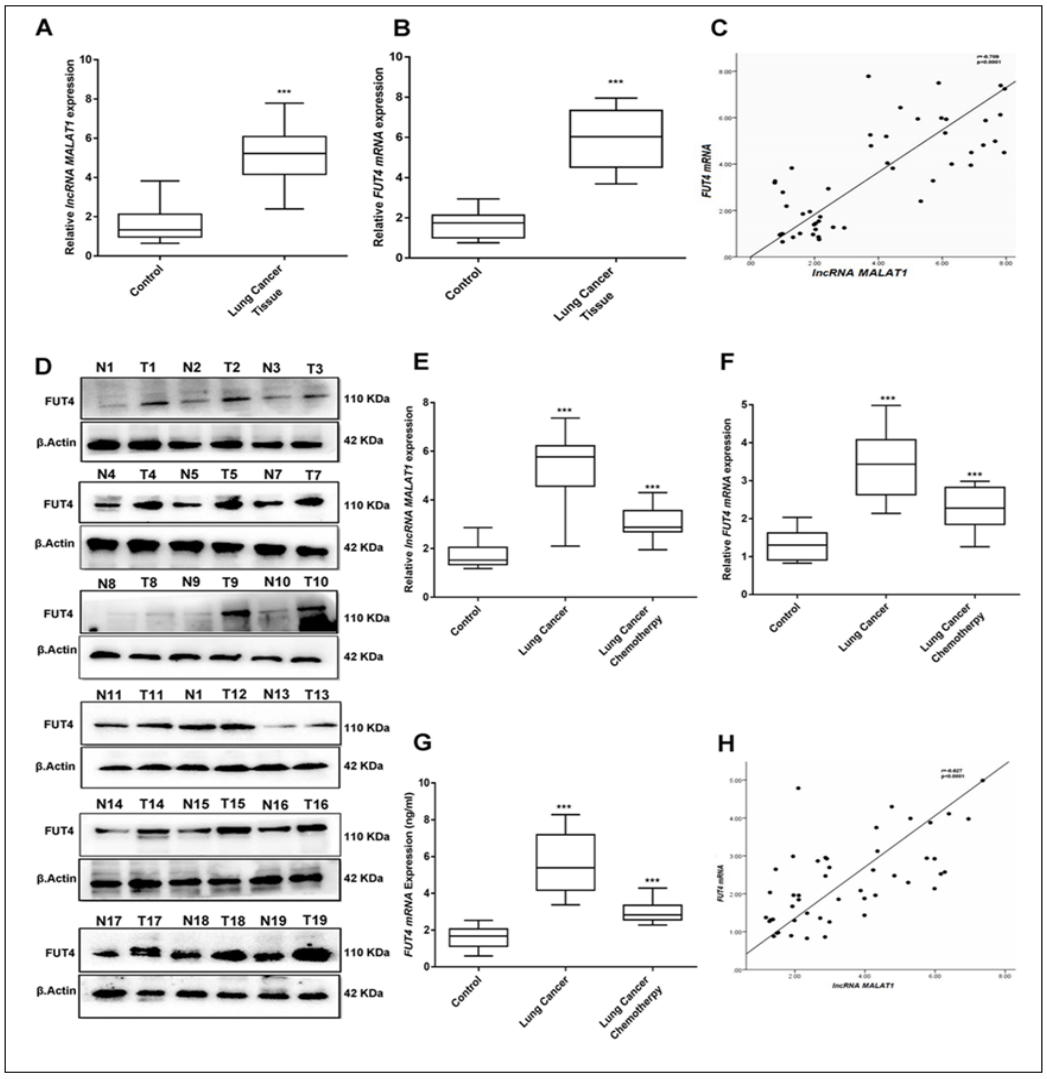


Figure 1. Correlation between *MALAT1* and *FUT4* Expression in Lung Cancer Tissues and Serum Samples. (A and B) Reverse transcription-quantitative polymerase chain reaction (RT-qPCR) analysis of metastasis-associated lung adenocarcinoma transcript 1 (*MALAT1*) and fucosyltransferase 4 (*FUT4*) expression in lung cancer tissues and matched adjacent tissues (n=19 biological replicates). Data are presented as mean ± SE. P = 0.023 for *MALAT1*; P = 0.017 for *FUT4* by paired Student's t-test. (C) Spearman's rank correlation between *MALAT1* and *FUT4* expression in tissue samples (n=19). r = 0.509; 95% confidence interval: 0.182–0.742; P = 0.008. (D) Western blot analysis of *FUT4* protein in lung cancer (T1–T19) and adjacent tissues (N1–N19); β-actin served as the loading control. Blots are representative of n=19 independent samples. Densitometric quantification (right panel) shows mean ± SE from three independent experiments. P = 0.015 vs. adjacent tissue by paired t-test. (E) *MALAT1* expression in serum from healthy controls (n=15), untreated lung cancer patients (n=20), and post-chemotherapy patients (n=15). Data are mean ± SE. P = 0.008 vs. control; P = 0.032 vs. untreated by one-way ANOVA with Tukey's post hoc test. (F and G) *FUT4* levels in serum determined by RT-qPCR and enzyme-linked immunosorbent assay (ELISA) in the same groups as in E. For RT-qPCR: P = 0.011 vs. control; P = 0.028 vs. untreated. For ELISA: P = 0.006 vs. control; P = 0.021 vs. untreated. (H) Correlation between *MALAT1* and *FUT4* expression in serum (n=50 samples). Spearman's r = 0.627; 95% CI: 0.432–0.768; P < 0.001. (I) *MALAT1* and *FUT4* expression levels in early-stage (I-II, n=10) and late-stage (III, n=9) non-small cell lung cancer (NSCLC) tumors from the tissue cohort. Data are mean ± SE. P = 0.009 for *MALAT1*; P = 0.013 for *FUT4* by unpaired t-test. These associations should be considered exploratory given the cohort size. Data are presented as the mean ± standard error (SE) from three independent experimental replicates. P<0.05, P<0.01 and P<0.001 vs. control/adjacent tissue. Statistical analysis was performed using paired or unpaired Student's t-test, one-way ANOVA with Tukey's post hoc test, or Spearman's rank correlation as appropriate.

(Figures 2C, 2D; P < 0.001 at day 4 for both cell lines), and significantly reduced clonogenic capacity in both cell lines (Figures 2E, 2F; P = 0.002 for A549; P = 0.004 for H1299). These functional assays were repeated in three independent biological replicates. Transwell assays further showed that si-*MALAT1* decreased the migratory and invasive capabilities of these cells compared to controls (Figures 2G–2J; P = 0.003 for A549 migration; P = 0.001 for A549 invasion; P = 0.005 for H1299 migration; P = 0.002 for H1299 invasion). Effect sizes (Cohen's d) for migration and invasion ranged from 1.8 to 2.4, indicating large effects. Cell counts were performed in ten random fields per membrane, and each experiment was conducted with n = 3 independent biological replicates. These data

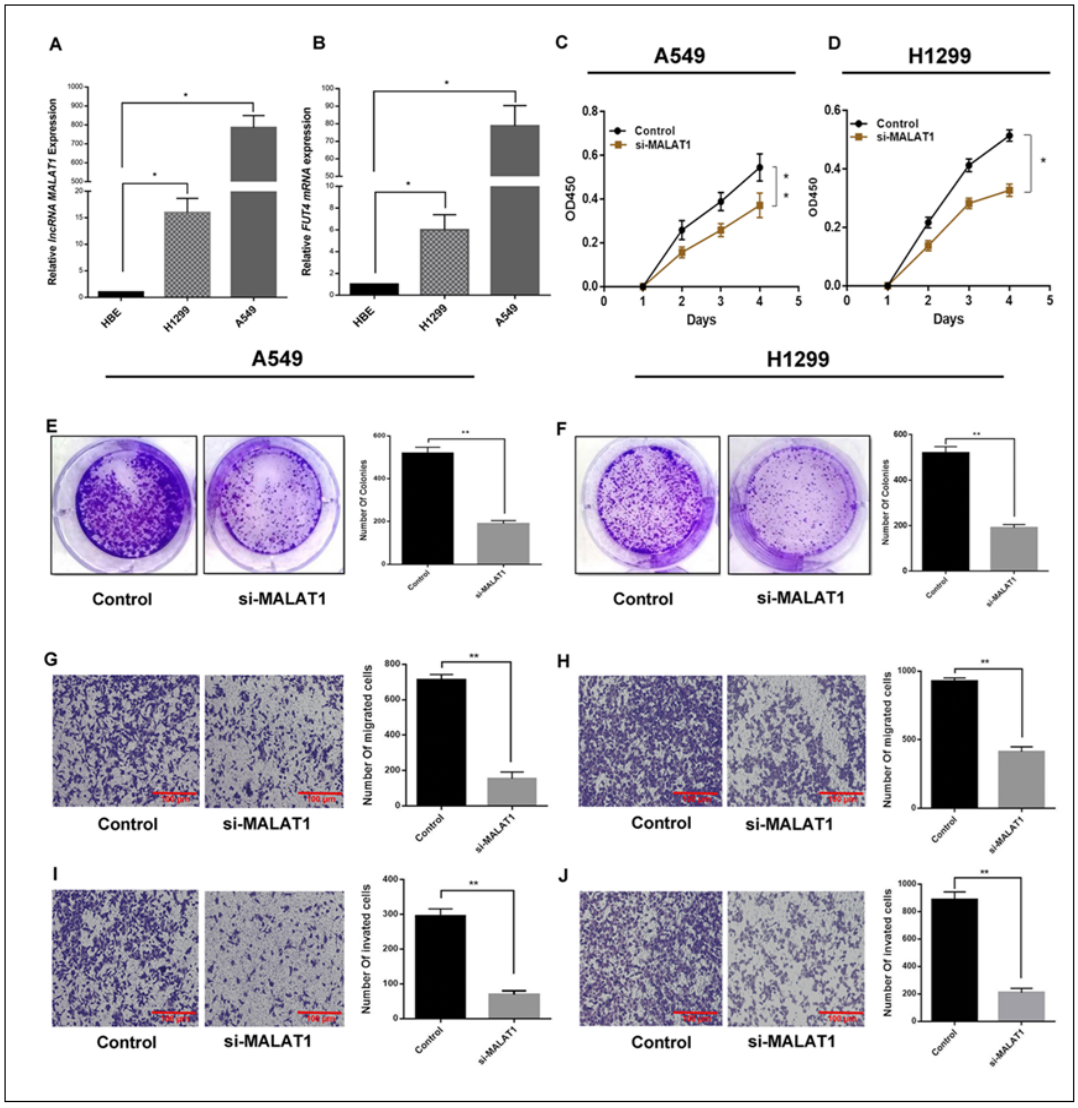


Figure 2. *MALAT1* Promotes Proliferation, Migration, and Invasion in A549 and H1299 Cells. (A and B) Relative *MALAT1* and *FUT4* expression in lung cancer cell lines vs. human bronchial epithelial (HBE) cells (n=3 independent experiments). Data are mean ± SE. P = 0.009 for A549 *MALAT1*; P = 0.013 for A549 *FUT4*; P = 0.006 for H1299 *MALAT1*; P = 0.011 for H1299 *FUT4* by one-way ANOVA with Dunnett's post hoc test vs. HBE. (C and D) Cell Counting Kit-8 (CCK-8) assay measuring cell viability over 4 days after si-*MALAT1* transfection; absorbance was measured at 450 nm (n=3 independent experiments, each with 6 technical replicates). Data are mean ± SE. P < 0.001 vs. control at day 4 for both cell lines by two-way ANOVA with Bonferroni post hoc test. (E and F) Colony formation of si-*MALAT1*-transfected cells stained with crystal violet after 12 days; quantified graphically (n=3 independent experiments). Data are mean ± SE. P = 0.002 for A549; P = 0.004 for H1299 by unpaired t-test. (G and H) Transwell migration assay with crystal violet-stained cells after 48 h incubation (1×10^5 cells); quantified from ten random fields per membrane by two independent blinded observers (n=3 independent experiments). Data are mean ± SE. P = 0.003 for A549; P = 0.005 for H1299 by unpaired t-test. Effect sizes (Cohen's d): 2.1 for A549, 1.9 for H1299. (I and J) Transwell invasion assay conducted under the same conditions (n=3 independent experiments). Data are mean ± SE. P = 0.001 for A549; P = 0.002 for H1299 by unpaired t-test. Effect sizes (Cohen's d): 2.4 for A549, 2.0 for H1299. Data are presented as the mean ± SE; P<0.01 vs. control by Student's t-test. Original magnification, x200.

confirm *MALAT1*'s role in promoting NSCLC cell growth and motility.

MALAT1 Regulates FUT4 Expression in Lung Cancer Cells

Silencing *MALAT1* resulted in a significant reduction in *MALAT1* transcript levels (Figures 3A, 3C; P = 0.003 for A549; P = 0.001 for H1299), along with downregulation of *FUT4* mRNA and protein expression (Figures 3B, 3D–3F; P = 0.007 for A549 *FUT4* mRNA; P = 0.005 for H1299 *FUT4* mRNA; P = 0.012 for A549 *FUT4* protein; P = 0.009 for H1299 *FUT4* protein) in A549 and H1299 cells. Immunofluorescence showed decreased *FUT4* expression following *MALAT1* knockdown, confirming *FUT4* as a downstream target of *MALAT1* regulation (Figures 3G, 3H; P = 0.002 for A549; P = 0.004 for H1299). All Western blot densitometry data were obtained from three independent biological experiments.

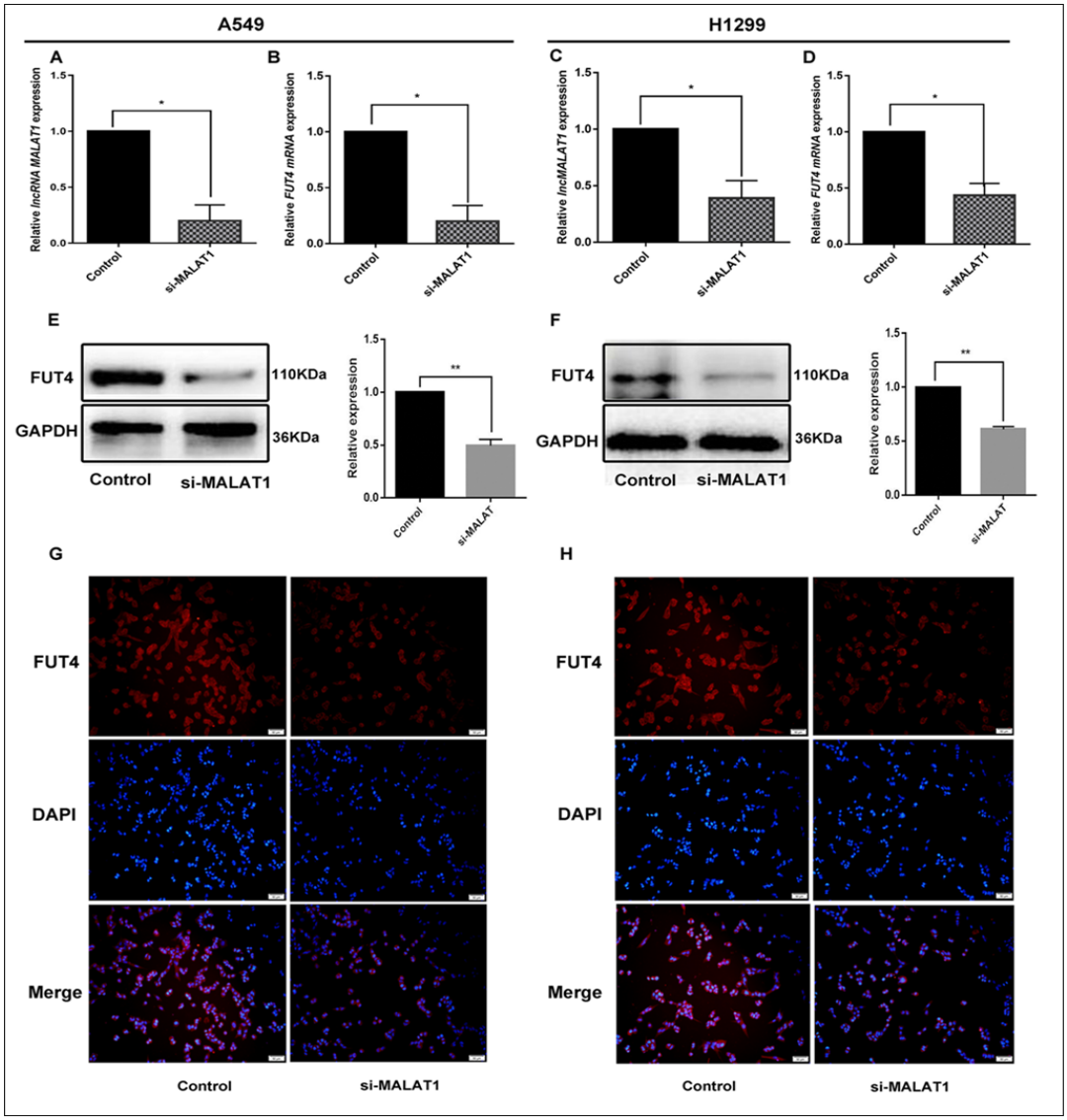


Figure 3. *MALAT1* Regulates *FUT4* Expression in Lung Cancer Cells. (A-D) RT-qPCR of *MALAT1* and FUT4 in si-*MALAT1*-transfected vs. control cells (n=3 independent experiments). Data are mean ± SE. For A549: P = 0.003 (*MALAT1*), P = 0.007 (*FUT4*). For H1299: P = 0.001 (*MALAT1*), P = 0.005 (*FUT4*) by unpaired t-test. (E-G) Representative western blots and densitometry showing *FUT4* protein expression after *MALAT1* knockdown (n=3 independent experiments); β-actin served as the loading control. Data are mean ± SE. P = 0.012 for A549; P = 0.009 for H1299 by unpaired t-test. (H) Immunofluorescence for *FUT4* (primary antibody 1:50; TRITC-conjugated secondary antibody 1:100) with DAPI nuclear staining. Fluorescence intensity was quantified from at least 100 cells per condition across three independent experiments using ImageJ. Data are mean ± SE. P = 0.002 for A549; P = 0.004 for H1299 by unpaired t-test. Data are presented as the mean ± SE; P<0.01 vs. control by Student's t-test. Original magnification, x400.

MALAT1-Mediated FUT4 Expression Enhances Proliferation and Invasion

Proliferation and colony formation were significantly reduced in cells transfected with si-*MALAT1* compared to controls (Figures 4A, 4B; P < 0.001 for both cell lines at day 4). Migration and invasion assays showed that si-*MALAT1* decreased NSCLC cell motility and invasiveness, effects that were partially but significantly rescued by *FUT4* overexpression via cDNA transfection (Figures 4C–4H; P < 0.05 for si-*MALAT1* vs. control; #P < 0.05 for si-*MALAT1+FUT4* vs. si-*MALAT1* alone). The partial rescue (approximately 60–70% restoration of baseline levels) suggests that additional molecular effectors may contribute to *MALAT1*-dependent phenotypes. Data points represent the mean ± SE of three independent biological experiments.

MALAT1 Enhances α1,3-Fucosylation of EGFR and Activates PI3K/Akt Signaling

Lectin blotting with Lotus Tetragonolobus Lectin (LTL) demonstrated that si-*MALAT1* reduced α1,3-fucosylation and Lewis Y (LeY) antigen levels on EGFR (Figures 5A, 5B; P = 0.008 for A549 LTL; P = 0.011 for A549 LeY; P = 0.006 for H1299 LTL; P = 0.013 for H1299 LeY). All immunoprecipitation experiments included IgG controls to confirm antibody specificity and input controls to verify equal protein loading. Total EGFR levels were used for normalization of glycosylation signals. Densitometric quantification was performed across three independent biological replicates. To further validate these

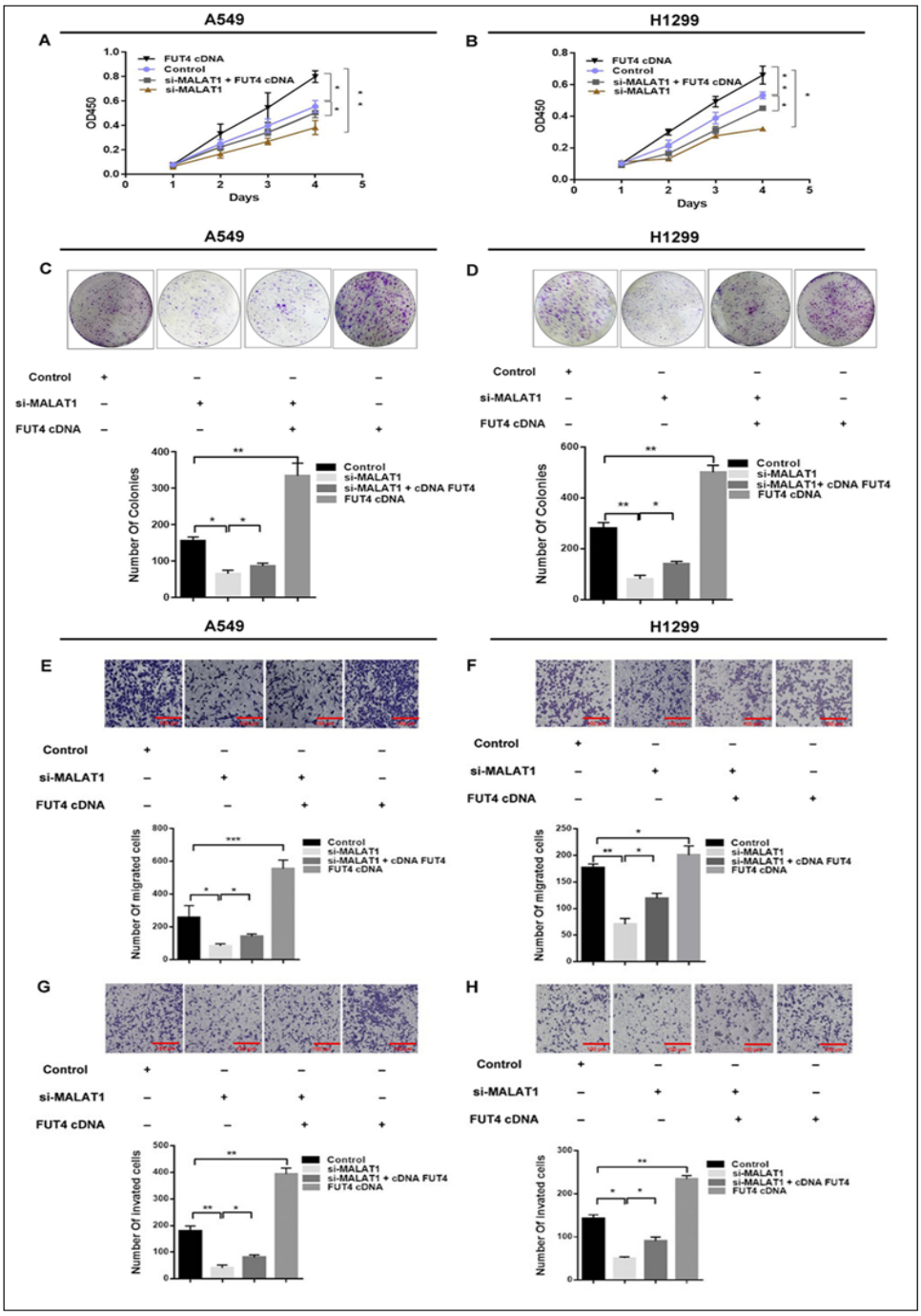


Figure 4. *MALAT1* Facilitates Lung Cancer Cell Proliferation and Invasion via *FUT4* Regulation. (A and B) CCK-8 assay of cell viability in control, si-*MALAT1*, *FUT4* cDNA, and combined transfectants (n=3 independent experiments, each with 6 technical replicates). Data are mean ± SE. P < 0.001 vs. control at day 4 for si-*MALAT1*; #P < 0.05 vs. si-*MALAT1* alone for si-*MALAT1+FUT4* by two-way ANOVA with Bonferroni post hoc test. (C and D) Colony formation assay after 14 days in the indicated groups (n=3 independent experiments). Data are mean ± SE. P < 0.01 vs. control; #P < 0.05 vs. si-*MALAT1* alone by one-way ANOVA with Tukey's post hoc test. (E and F) Transwell migration of treated cells; quantification from ten random fields per membrane by two independent blinded observers (n=3 independent experiments). Data are mean ± SE. P < 0.01 vs. control; #P < 0.05 vs. si-*MALAT1* alone by one-way ANOVA with Tukey's post hoc test. The partial rescue (approximately 60-70% restoration) suggests additional effectors may contribute to *MALAT1*-dependent phenotypes. (G and H) Transwell invasion assay with the same groups and quantification (n=3 independent experiments). Data are mean ± SE. P < 0.01 vs. control; #P < 0.05 vs. si-*MALAT1* alone by one-way ANOVA with Tukey's post hoc test. Data are presented as the mean ± SE; P<0.05 vs. control; #P<0.05 vs. si-*MALAT1* group by one-way ANOVA followed by Tukey's post hoc test. Original magnification, x1000.

findings, orthogonal confirmation was performed using LTL lectin blotting following EGFR immunoprecipitation (Figure 5C), which confirmed reduced α1,3-fucosylation of EGFR upon *MALAT1* knockdown. Immunoprecipitation and immunoblotting analyses confirmed diminished LeY-modified EGFR following *MALAT1* knockdown (Figures 5C, 5D). Uncropped, full-length Western blot images are provided in Supplementary Figure 1. Treatment with LeY antibodies or EGFR inhibitors suppressed EGFR phosphorylation, underscoring the importance of

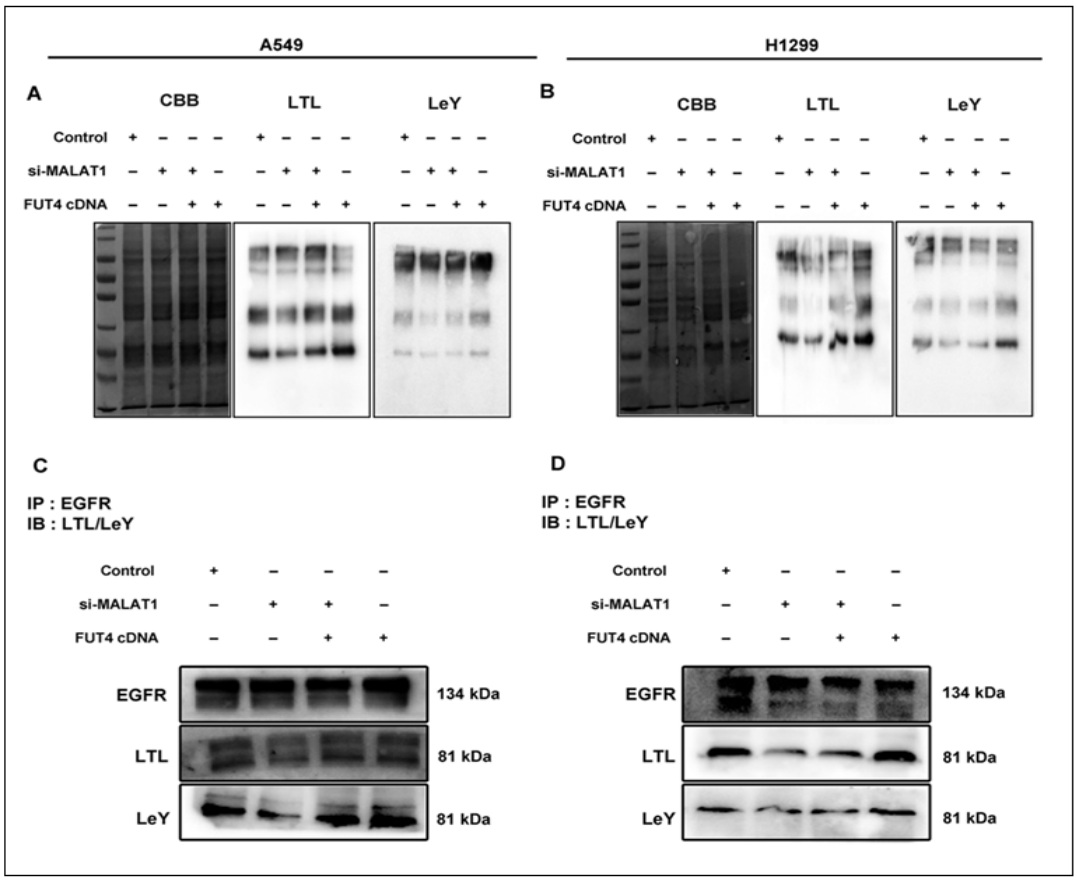


Figure 5. *MALAT1* Enhances α1,3-fucosylation, LeY Antigen Biosynthesis, and EGFR phosphorylation. (A and B) Lectin blot assays for α1,3-fucosylation (LTL lectin) and Lewis Y (LeY) antigen (anti-LeY IgM) in control and transfected lung cancer cells after 48 h. All immunoprecipitation experiments included normal rabbit IgG as a negative control to confirm antibody specificity. Input controls show total EGFR levels used for normalization. Densitometric quantification (right panels) was performed across three independent biological replicates. Coomassie brilliant blue staining served as the loading control. Data are mean ± SE. For A549 LTL: P = 0.008; A549 LeY: P = 0.011; H1299 LTL: P = 0.006; H1299 LeY: P = 0.013 by unpaired t-test. (C and D) Immunoprecipitation and western blot detecting α1,3-fucosylation and LeY on epidermal growth factor receptor (EGFR) in A549 and H1299 cells. To confirm specificity, orthogonal validation was performed using LTL lectin blotting following EGFR immunoprecipitation (upper panels). IgG control lanes demonstrate antibody specificity. Total EGFR was used for normalization. Densitometric quantification (right panels) from three independent experiments is shown. Data are mean ± SE. P < 0.05, P < 0.01 vs. control by unpaired t-test. Experiments were performed in triplicate. Uncropped, full-length Western blot images are provided in Supplementary Figure 1.

α1,3-fucosylation in receptor activation. Western blot analyses revealed that *MALAT1* knockdown decreased phosphorylation of PI3K, PDK, and Akt, effects reversed by *FUT4* overexpression (Figures 6A, 6B; P < 0.05 for all phosphorylated proteins in si-*MALAT1* vs. control; #P < 0.05 for si-*MALAT1+FUT4* vs. si-*MALAT1* alone). Effect sizes (η^2) for pathway activation ranged from 0.32 to 0.48, indicating large effects. These results support that *MALAT1* regulates the PI3K/Akt pathway, a critical driver of cell survival and proliferation, in a *FUT4*-dependent manner. All representative blots are from experiments repeated at least three times with consistent results.

Discussion

This study clarifies the role of lncRNA *MALAT1* in promoting proliferation and metastasis in NSCLC by regulating fucosyltransferase 4 (*FUT4*), thereby increasing α1,3-fucosylation and Lewis Y (LeY) biosynthesis on glycoproteins, particularly EGFR. Our findings highlight the potential of *MALAT1* and *FUT4* as diagnostic biomarkers and therapeutic targets in lung cancer. Dysregulated lncRNAs are widely recognised as critical drivers of tumour progression and epithelial-mesenchymal transition (EMT) in various cancers [25, 26]. *MALAT1*, which is extensively overexpressed in numerous malignancies, orchestrates key processes such as cell proliferation, invasion, and metastasis [27, 28]. In line with previous reports, we observed elevated *MALAT1* levels in both serum and tumour tissues from NSCLC patients compared to healthy controls [25, 28]. Similarly, *FUT4* overexpression enhances oncogenic traits in several cancer types and showed a positive correlation with *MALAT1* in our NSCLC cohort, further supporting their cooperative role in tumour biology [29, 30].

Importantly, our analysis showed that high levels of *MALAT1* and *FUT4* are significantly associated with advanced TNM stages and lymph node metastasis in this

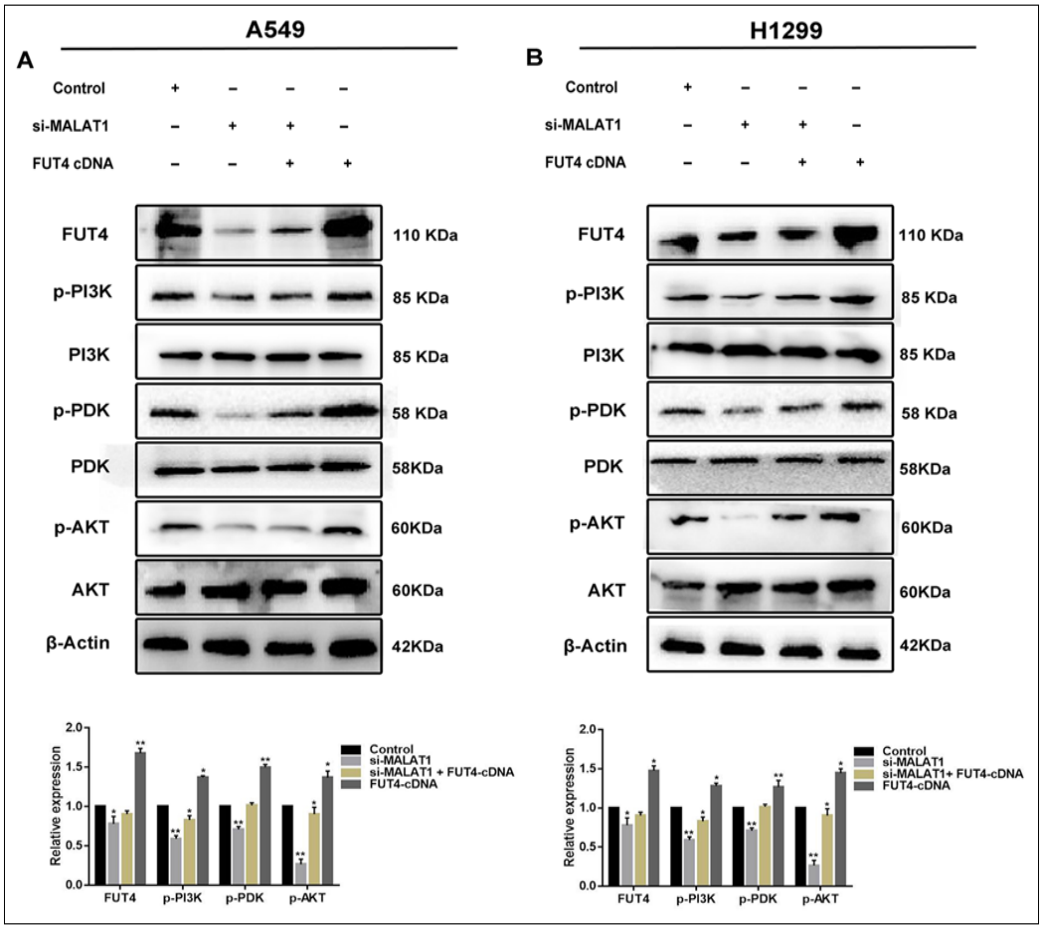


Figure 6. *MALAT1* Regulates *FUT4* through PI3K/Akt Pathway Activation. (A and B) Western blot and densitometry of phosphorylated (p-) phosphatidylinositol 3-kinase (PI3K), p-PDK, and p-Akt in control and transfected A549 and H1299 cells. β-actin served as the loading control. Densitometric quantification (right panels) from three independent experiments is shown. Data are mean ± SE. For all phosphorylated proteins: $P < 0.05$ vs. control; #$P < 0.05$ vs. si-*MALAT1* alone by one-way ANOVA followed by Tukey's post hoc test. Effect sizes (η^2) ranged from 0.32 to 0.48, indicating large effects. Data are presented as the mean ± SE from three independent experiments; $P<0.05$ vs. control; #$P<0.05$ vs. si-*MALAT1* group by one-way ANOVA followed by Tukey's post hoc test.

cohort. However, these findings should be considered exploratory due to the modest sample size and require validation in larger, independent cohorts. Notably, chemotherapy treatment was associated with reduced *MALAT1* and *FUT4* expression, suggesting a potential link with treatment response that warrants prospective validation.

Our investigation focused on lung cancer cell lines A549 and H1299, which are characterised by high *MALAT1* and *FUT4* expression, consistent with a metastatic phenotype. *MALAT1* knockdown via siRNA significantly inhibited cell proliferation, colony formation, migration, and invasion, mirroring the effects of *FUT4* silencing reported in other malignancies [23, 28, 31, 32].

A key finding of our study is that the oncogenic effects of *MALAT1* are, at least in part, mediated through its regulation of *FUT4*, as *FUT4* overexpression partially rescued the phenotypic deficits induced by *MALAT1* silencing. The partial nature of this rescue suggests that additional molecular effectors may contribute to *MALAT1*-dependent phenotypes, a complexity that warrants further investigation.

The precise molecular mechanism by which *MALAT1* regulates *FUT4* expression also warrants further investigation. While our study establishes a functional regulatory relationship, the direct interaction mechanism remains to be elucidated. Based on findings in colorectal cancer, where *MALAT1* has been shown to upregulate *FUT4* by sponging miR-26a and miR-26b [21], it is conceivable that a similar ceRNA mechanism may operate in NSCLC. However, this remains a hypothesis that requires direct experimental validation through approaches such as RNA immunoprecipitation (RIP), luciferase reporter assays, and miRNA gain- or loss-of-function studies. Future work in our laboratory will focus on systematically investigating this potential mechanism, including bioinformatic prediction of miRNA binding sites and experimental validation of *MALAT1*–miRNA–*FUT4* interactions.

Furthermore, the *MALAT1-FUT4* axis is closely linked to STAT3 activation pathways, which are extensively implicated in cancer progression and drug resistance [23, 33-36]. In cisplatin-resistant A549 cells, elevated *MALAT1* correlates with STAT3 activation and *FUT4* expression, while *MALAT1* knockdown reduces both [35,37]. This suggests that *MALAT1* may promote *FUT4* expression

and drug resistance partly through STAT3 modulation, a potential intersection that enhances our understanding of the regulatory network.

Aberrant fucosylation is a recognised hallmark of malignancy [38]. Our data, showing decreased tumour aggressiveness upon *MALAT1* knockdown and reduced *FUT4* expression, corroborate previous findings that limiting fucosyltransferase activity suppresses tumour malignancy [39]. While our study focused on *FUT4* as a key downstream effector of *MALAT1*, it is important to recognise that fucosylation is a complex process involving multiple fucosyltransferases with distinct substrate specificities and linkage preferences. *FUT4* specifically catalyses α1,3-fucosylation, contributing to LeY antigen synthesis. However, other family members, including FUT6 (also an α1,3-fucosyltransferase), FUT8 (an α1,6-fucosyltransferase involved in core fucosylation), and FUT3/5 (which generate Lewis antigens), may also contribute to the overall fucosylation landscape in NSCLC and could potentially interact with or compensate for *FUT4* modulation. Preliminary analysis of public NSCLC transcriptomic datasets (data not shown) suggests coordinated regulation of multiple fucosyltransferases. Future studies should determine whether *MALAT1* selectively regulates *FUT4* or has broader effects on the fucosyltransferase network. Our results show that *MALAT1* silencing reduces LeY biosynthesis on EGFR. The LeY antigen on EGFR promotes receptor dimerisation and activation, initiating proliferative and invasive signalling cascades such as the PI3K/Akt pathway [40]. Thus, the reduction in LeY-modified EGFR after *MALAT1* knockdown likely leads to PI3K/Akt signalling inactivation, thereby suppressing lung cancer progression. Blockade of LeY has been shown to impair EGFR function and reduce tumour cell proliferation [41], consistent with our mechanistic observations.

Strengths, Limitations, and Future Perspectives

A strength of this study is its novel investigation of *MALAT1*'s regulation of *FUT4* in lung cancer, its association with chemotherapy response, and the potential of both molecules as biomarkers. However, several limitations should be noted. Firstly, the tissue cohort size (n = 19) is relatively small, which may reduce statistical power for detecting subtle associations and prevents robust multivariable analyses. Although our findings reached statistical significance, they should be regarded as exploratory and hypothesis-generating. Validation in larger, multi-centre cohorts is necessary to confirm the observed correlations and to establish the clinical utility of *MALAT1* and *FUT4* as biomarkers. We are currently initiating a multi-centre collaboration to collect an independent validation cohort of approximately 100 NSCLC patients, which will allow for more robust statistical modelling and subgroup analyses.

Secondly, all our mechanistic data are derived from *In vitro* experiments. The absence of in vivo validation using animal models, such as xenograft or orthotopic studies, is a significant limitation that we plan to address in future research to confirm the biological role of the *MALAT1*/*FUT4* axis within the tumour microenvironment. Such studies would also enable evaluation of therapeutic targeting strategies in a physiologically relevant context.

Thirdly, although we established that *MALAT1* regulates *FUT4* expression, the direct molecular mechanism– whether through transcriptional activation, miRNA sponging, or signalling intermediates such as STAT3 remains to be elucidated. Future work should aim to decode this precise regulatory network, including the potential involvement of other downstream effectors such as the mTOR axis.

Fourthly, the assessment of EGFR glycosylation in this study relies primarily on immunoprecipitation followed by lectin blotting and LeY immunodetection. While these approaches provide evidence of glycosylation status, they do not offer detailed structural information about glycan composition. Future studies employing mass spectrometry-based glycoproteomics would provide complementary, higher-resolution characterisation of EGFR glycosylation patterns modulated by the *MALAT1*/*FUT4* axis.

Finally, regarding translational potential, the identification of the *MALAT1*/*FUT4*/EGFR axis as a driver of NSCLC progression raises intriguing therapeutic possibilities. *MALAT1*-targeting strategies, including antisense oligonucleotides and small molecule inhibitors, are under active investigation in preclinical cancer models. Similarly, interference with LeY-mediated EGFR glycosylation using blocking antibodies or fucosylation inhibitors represents a conceptually attractive approach. However, these therapeutic implications remain speculative and are based entirely on *In vitro* observations.

Critical next steps include: (i) validation in orthotopic and patient-derived xenograft mouse models to establish in vivo efficacy and safety; (ii) investigation of potential on-target and off-tumour effects, given the physiological roles of *MALAT1* and *FUT4* in normal tissues; and (iii) evaluation of combinatorial approaches with existing standard-of-care therapies. Without such rigorous preclinical validation, translation to clinical applications remains premature.

In Conclusion, this study provides evidence that *MALAT1* is a central modulator of NSCLC progression, acting through upregulation of *FUT4*, promotion of EGFR α1,3-fucosylation, and activation of the PI3K/Akt pathway. This molecular axis underpins key malignant phenotypes, including enhanced proliferation, migration, and colony formation, and may contribute to therapeutic resistance. While further validation in larger cohorts and in vivo models is required, targeting the *MALAT1*-*FUT4*-PI3K/Akt axis represents a promising strategy for the diagnosis and treatment of NSCLC. Future investigations should focus on validating these findings in larger clinical cohorts and in vivo models, elucidating the precise regulatory mechanism linking *MALAT1* to *FUT4*, and exploring the therapeutic efficacy of disrupting this oncogenic network.

Acknowledgements

Conflicts of Interest Statement

The authors declare that they have no competing interests. No financial or non-financial conflicts of interest exist related to this work.

Ethics Approval and Consent to Participate

The study was conducted in accordance with the Declaration of Helsinki and approved by the Ethics Committee of the First Affiliated Hospital of Dalian Medical University (approval no. YJ-KY-FB-2019-32; approval date: January 15, 2019). Written informed consent was obtained from all participating patients for the collection of medical data, tissue specimens, and serum samples prior to enrollment in the study.

Patient Consent for Publication

Written informed consent was obtained from all patients for publication of this study and any accompanying images. The consent documents are available for editorial review upon request.

Data Availability Statement

The datasets generated and analyzed during the current study are available in the Mendeley Data repository:

Alshwmi, Mohammed; Li, Shijun; Ahmed, Faisal; Saleem, Muhammad; Juebin, Gu; Yingxin, Wang; Badheeb, Mohamed (2024). "Long non-coding RNA *MALAT1* promotes the proliferation and metastasis of lung cancer by regulating *FUT4* and α1,3-fucosylated glycans mediated via the PI3K/Akt signaling pathway." Mendeley Data, V1, doi: 10.17632/275n44hk5p.1.

Accessible at: https://data.mendeley.com/datasets/275n44hk5p/1

Additional data supporting the findings of this study are available from the corresponding author upon reasonable request.

Funding Statement

This research did not receive any specific grant from funding agencies in the public, commercial, or not-for-profit sectors. All expenses were covered by institutional resources of Dalian Medical University.

Author Contributions

Mohammed Alshwmi and Shijun Li contributed equally to this work. Mohammed Alshwmi and Shijun Li were responsible for study conception, experimental design, data interpretation, and manuscript drafting. Muhammad Saleem, Gu Juebin, and Wang Yingxin performed the experiments, acquired data, and conducted statistical analyses. Mohamed Badheeb and Faisal Mohammed Ahmed contributed to clinical sample collection, patient data management, and manuscript revision. Mohammed Alshwmi and Faisal Mohammed Ahmed contributed to the study conception and critically reviewed the manuscript for important intellectual content. All authors read and approved the final manuscript and agree to be accountable for all aspects of the work, ensuring that questions related to the accuracy or integrity of any part of the work are appropriately investigated and resolved.

Use of Artificial Intelligence Tools

DeepSeek (developed by DeepSeek AI) was utilized for English language editing of the manuscript to improve clarity, grammar, and style. The AI tool assisted in refining sentence structure and enhancing overall readability while preserving the scientific content and meaning. The authors take full responsibility for the scientific content, originality, and interpretation presented in this manuscript, and have thoroughly reviewed and approved all AI-assisted edits.

Originality Declaration for Figures

All figures included in this manuscript are original and have been created by the authors specifically for the purposes of this study. No previously published or copyrighted images have been used. The authors confirm that all graphical elements, illustrations, and visual materials were generated from the data obtained in the course of this research or designed uniquely for this manuscript.

References

1. Molina JR, Yang P, Cassivi SD, Schild SE, Adjei AA. Non-small cell lung cancer: epidemiology, risk factors, treatment, and survivorship. Mayo Clinic Proceedings. 2008 05;83(5):584-594. https://doi.org/10.4065/83.5.584
2. Sung H, Ferlay J, Siegel RL, Laversanne M, Soerjomataram I, Jemal A, Bray F. Global Cancer Statistics 2020: GLOBOCAN Estimates of Incidence and Mortality Worldwide for 36 Cancers in 185 Countries. CA: a cancer journal for clinicians. 2021 05;71(3):209-249. https://doi.org/10.3322/caac.21660
3. Huang Q, Li Y, Huang Y, Wu J, Bao W, Xue C, Li X, et al. Advances in molecular pathology and therapy of non-small cell lung cancer. Signal Transduction and Targeted Therapy. 2025 06 15;10(1):186. https://doi.org/10.1038/s41392-025-02243-6
4. Haggstrom L, Chan WY, Nagrial A, Chantrill LA, Sim H, Yip D, Chin V. Chemotherapy and radiotherapy for advanced pancreatic cancer. The Cochrane Database of Systematic Reviews. 2024 Dec 05;12(12):CD011044. https://doi.org/10.1002/14651858.CD011044.pub3
5. Zappa C, Mousa SA. Non-small cell lung cancer: current treatment and future advances. Translational Lung Cancer Research. 2016 06;5(3):288-300. https://doi.org/10.21037/tlcr.2016.06.07
6. Cuevas-Diaz Duran R, Wei H, Kim DH, Wu JQ. Invited Review: Long non-coding RNAs: important regulators in the development, function and disorders of the central nervous system. Neuropathology and Applied Neurobiology. 2019 Oct;45(6):538-556. https://doi.org/10.1111/nan.12541
7. Liu L, Yang L, Li H, Shang T, Liu L. The tumor microenvironment in lung cancer: Heterogeneity, therapeutic resistance and emerging treatment strategies (Review). International Journal of Oncology. 2026 01;68(1):11. https://doi.org/10.3892/ijo.2025.5824
8. Xi Z, Dai R, Ze Y, Jiang X, Liu M, Xu H. Traditional Chinese medicine in lung cancer treatment. Molecular Cancer. 2025 02 26;24(1):57. https://doi.org/10.1186/s12943-025-02245-6

9. Munkley J, Elliott DJ. Hallmarks of glycosylation in cancer. Oncotarget. 2016 06 07;7(23):35478-35489. https://doi.org/10.18632/oncotarget.8155
10. Toraih EA, Ellawindy A, Fala SY, Al Ageeli E, Gouda NS, Fawzy MS, Hosny S. Oncogenic long noncoding RNA *MALAT1* and HCV-related hepatocellular carcinoma. Biomedicine & Pharmacotherapy = Biomedecine & Pharmacotherapie. 2018 06;102:653-669. https://doi.org/10.1016/j.biopha.2018.03.105
11. He X, Yan Q, Kuang G, Wang Y, Cao P, Ou C. Metastasis-associated lung adenocarcinoma transcript 1 regulates tumor progression: old wine in a new bottle. Journal of Thoracic Disease. 2018 04;10(Suppl 9):S1088-S1091. https://doi.org/10.21037/jtd.2018.04.13
12. Arun G, Aggarwal D, Spector DL. *MALAT1* Long Non-Coding RNA: Functional Implications. Non-coding RNA. 2020 06 03;6(2):22. https://doi.org/10.3390/ncrna6020022
13. Amodio N, Raimondi L, Juli G, Stamato MA, Caracciolo D, Tagliaferri P, Tassone P. *MALAT1*: a druggable long non-coding RNA for targeted anti-cancer approaches. Journal of Hematology & Oncology. 2018 05 08;11(1):63. https://doi.org/10.1186/s13045-018-0606-4
14. Lu H, Lin S, Weng RR, Juan Y, Chen Y, Hou H, Hung Z, Oswita GA, et al. Fucosyltransferase 4 shapes oncogenic glycoproteome to drive metastasis of lung adenocarcinoma. EBioMedicine. 2020 07;57:102846. https://doi.org/10.1016/j.ebiom.2020.102846
15. Yang X, Liu S, Yan Q. Role of fucosyltransferase IV in epithelial-mesenchymal transition in breast cancer cells. Cell Death & Disease. 2013 07 25;4(7):e735. https://doi.org/10.1038/cddis.2013.241
16. Gutschner T, Hämmerle M, Eissmann M, Hsu J, Kim Y, Hung G, Revenko A, et al. The noncoding RNA *MALAT1* is a critical regulator of the metastasis phenotype of lung cancer cells. Cancer Research. 2013 02 01;73(3):1180-1189. https://doi.org/10.1158/0008-5472.CAN-12-2850
17. Hussein MA, Valinezhad K, Adel E, Munirathinam G. MALAT-1 Is a Key Regulator of Epithelial-Mesenchymal Transition in Cancer: A Potential Therapeutic Target for Metastasis. Cancers. 2024 01 04;16(1):234. https://doi.org/10.3390/cancers16010234
18. Xu D, Wang W, Wang D, Ding J, Zhou Y, Zhang W. Long noncoding RNA MALAT-1: A versatile regulator in cancer progression, metastasis, immunity, and therapeutic resistance. Non-coding RNA research. 2024 06;9(2):388-406. https://doi.org/10.1016/j.ncrna.2024.01.015
19. Keeley TS, Yang S, Lau E. The Diverse Contributions of Fucose Linkages in Cancer. Cancers. 2019 08 24;11(9):1241. https://doi.org/10.3390/cancers11091241
20. Lin W, Lin Y, Shi G, Chang C, Wu H. Lewisy promotes migration of oral cancer cells by glycosylation of epidermal growth factor receptor. PloS One. 2015;10(3):e0120162. https://doi.org/10.1371/journal.pone.0120162
21. Xu J, Xiao Y, Liu B, Pan S, Liu Q, Shan Y, Li S, et al. Exosomal *MALAT1* sponges miR-26a/26b to promote the invasion and metastasis of colorectal cancer via *FUT4* enhanced fucosylation and PI3K/Akt pathway. Journal of Experimental & Clinical Cancer Research : CR. 2020 03 24;39:54. https://doi.org/10.1186/s13046-020-01562-6
22. Du B, Wang J, Zang S, Mao X, Du Y. Long non-coding RNA *MALAT1* suppresses the proliferation and migration of endothelial progenitor cells in deep vein thrombosis by regulating the Wnt/β-catenin pathway. Experimental and Therapeutic Medicine. 2020 Oct;20(4):3138-3146. https://doi.org/10.3892/etm.2020.9066
23. Yu L, Shao X, Huo L, Zhang T. Long Non-Coding RNA (lncRNA) Metastasis-Associated Lung Adenocarcinoma Transcript 1 (*MALAT1*) Promotes Cell Proliferation and Migration by Regulating miR-143-3p and MAGE Family Member A9 (MAGEA9) in Oral Squamous Cell Carcinoma. Medical Science Monitor: International Medical Journal of Experimental and Clinical Research. 2020 09 03;26:e924187. https://doi.org/10.12659/MSM.924187
24. Mishra M, Tiwari S, Gomes AV. Protein purification and analysis: next generation Western blotting techniques. Expert Review of Proteomics. 2017 Nov;14(11):1037-1053. https://doi.org/10.1080/14789450.2017.1388167
25. Tahernejad M, Hamidiazar S, Jamshidian F. Non-coding RNAs as non-invasive diagnostic biomarkers for lung cancer %J Human Genetics and Genomics. 2023;7.
26. Chen M, Feng X, Liu C, Huang Y, Su L, Li X, Zhu J. Diagnostic value of exosome-derived lncRNA PITPNA-AS1 in lung cancer. Frontiers in Immunology. 2025;16:1539557. https://doi.org/10.3389/fimmu.2025.1539557
27. Slack FJ, Chinnaiyan AM. The Role of Non-coding RNAs in Oncology. Cell. 2019 Nov 14;179(5):1033-1055. https://doi.org/10.1016/j.cell.2019.10.017
28. Li W, Li W, Xu Z. LncRNA MIR99AHG serves as a diagnostic marker for early lung cancer and regulates cancer cell growth and metastasis via miR-194-5p. Discover Oncology. 2025 06 10;16(1):1050. https://doi.org/10.1007/s12672-025-02896-3
29. Bakrim S, Fessikh ME, Elhrech H, Omari NE, Amanullah M, Ming LC, Moshawih S, Bouyahya A. Targeting inflammation in cancer therapy: from mechanistic insights to emerging therapeutic approaches. Journal of Translational Medicine. 2025 05 26;23(1):588. https://doi.org/10.1186/s12967-025-06583-3
30. Xie Y, Zhang Y, Du L, Jiang X, Yan S, Duan W, Li J, et al. Circulating long noncoding RNA act as potential novel biomarkers for diagnosis and prognosis of non-small cell lung cancer. Molecular Oncology. 2018 05;12(5):648-658. https://doi.org/10.1002/1878-0261.12188
31. Li J, Dhilipkannah P, Holden VK, Sachdeva A, Todd NW, Jiang F. Dysregulation of lncRNA *MALAT1* Contributes to Lung Cancer in African Americans by Modulating the Tumor Immune Microenvironment. Cancers. 2024 05 15;16(10):1876. https://doi.org/10.3390/cancers16101876
32. Roh J, Kim B, Im M, Jang W, Chae Y, Kang J, Youn B, Kim W. *MALAT1*-regulated gene expression profiling in lung cancer cell lines. BMC cancer. 2023 09 04;23(1):818. https://doi.org/10.1186/s12885-023-11347-7
33. Peng N, He J, Li J, Huang H, Huang W, Liao Y, Zhu S. Long noncoding RNA *MALAT1* inhibits the apoptosis and autophagy of hepatocellular carcinoma cell by targeting the microRNA-146a/PI3K/Akt/mTOR axis. Cancer Cell International. 2020;20:165. https://doi.org/10.1186/s12935-020-01231-w
34. Zheng Q, Zhang D, Yang YU, Cui X, Sun J, Liang C, Qin H, et al. MicroRNA-200c impairs uterine receptivity formation by targeting *FUT4* and α1,3-fucosylation. Cell Death and Differentiation. 2017 Dec;24(12):2161-2172. https://doi.org/10.1038/cdd.2017.136
35. Yang P, Liu L, Li E, Xu L. STAT3, the Challenge for Chemotherapeutic and Radiotherapeutic Efficacy. Cancers. 2020 08 30;12(9):2459. https://doi.org/10.3390/cancers12092459
36. Ding Y, Zhen Z, Nisar MA, Ali F, Din RU, Khan M, Mughal TA, et al. Sesquiterpene Lactones Attenuate Paclitaxel Resistance Via Inhibiting *MALAT1*/STAT3/ *FUT4* Axis and P-Glycoprotein Transporters in Lung Cancer Cells. Frontiers in Pharmacology. 2022;13:795613. https://doi.org/10.3389/fphar.2022.795613

37. Tano K, Mizuno R, Okada T, Rakwal R, Shibato J, Masuo Y, Ijiri K, Akimitsu N. MALAT-1 enhances cell motility of lung adenocarcinoma cells by influencing the expression of motility-related genes. FEBS letters. 2010 Nov 19;584(22):4575-4580. https://doi.org/10.1016/j.febslet.2010.10.008
38. Hu L, Tang J, Huang X, Zhang T, Feng X. Hypoxia exposure upregulates MALAT-1 and regulates the transcriptional activity of PTB-associated splicing factor in A549 lung adenocarcinoma cells. Oncology Letters. 2018 07;16(1):294-300. https://doi.org/10.3892/ol.2018.8637
39. Carrascal MA, Silva M, Ramalho JS, Pen C, Martins M, Pascoal C, Amaral C, et al. Inhibition of fucosylation in human invasive ductal carcinoma reduces E-selectin ligand expression, cell proliferation, and ERK1/2 and p38 MAPK activation. Molecular Oncology. 2018 05;12(5):579-593. https://doi.org/10.1002/1878-0261.12163
40. Seres M, Spacayova K, Sulova Z, Spaldova J, Breier A, Pavlikova L. Dynamic Multilevel Regulation of EGFR, KRAS, and MYC Oncogenes: Driving Cancer Cell Proliferation Through (Epi)Genetic and Post-Transcriptional/Translational Pathways. Cancers. 2025 01 14;17(2):248. https://doi.org/10.3390/cancers17020248
41. Mascia F, Schloemann DT, Cataisson C, McKinnon KM, Krymskaya L, Wolcott KM, Yuspa SH. Cell autonomous or systemic EGFR blockade alters the immune-environment in squamous cell carcinomas. International Journal of Cancer. 2016 Dec 01;139(11):2593-2597. https://doi.org/10.1002/ijc.30376

This work is licensed under a Creative Commons Attribution-Non Commercial 4.0 International License.